Micromechanical Interactions in a Superduplex Stainless Steel Subjected to Low Cycle Fatigue Loading

R. Lin Peng, G. Chai, N. Jia, Y. D. Wang and S. Johansson

R. Lin Peng, G. Chai, N. Jia, Y. D. Wang and S. Johansson, Micromechanical Interactions in a Superduplex Stainless Steel Subjected to Low Cycle Fatigue Loading, 2008, Fatigue and Fracture of Engineering Materials and Structures, (31), 10, 892-901.
http://dx.doi.org/10.1111/j.1460-2695.2008.01277.x.

MICROMECHANICAL INTERACTIONS IN A SUPERDUPLEX STAINLESS STEEL SUBJECTED TO LOW CYCLE FATIGUE LOADING

R. Lin Peng[1,*], G. Chai[2], N. Jia[3], Y. D. Wang[3], S. Johansson[1]

[1]Department of Management and Engineering, Linköping University, S-58183 Linköping, Sweden

[2]Sandvik Materials Technology, R&D, SFM, S-811 81 Sandviken, Sweden

[3]School of Materials and Metallurgy, Northeastern University, Shenyang 110004, China

Micromechanical interactions in an austenitic-ferritic SAF 2507 steel under low cycle fatigue loading was studied by experiment and simulation. Neutron diffraction measurements of residual lattice strains were made on specimens unloaded from different cyclic deformation stages, namely cyclic hardening, softening and saturation. With self-consistent modelling, the micromechanical behaviour of the constituent phases was studied for the first loading cycle. The evolution of the residual lattice strain distributions with cyclic loading and the development of phase stresses have been analyzed with respect to the initial residual stress field and the different mechanical properties of the constituent phases.

Keywords: duplex stainless steel, low cycle fatigue, micromechanical behaviour, neutron diffraction, VPSC simulation

INTRODUCTION

Superduplex stainless steels (SDSSs) are a new generation of austenitic-ferritic stainless steels with a higher alloying content than the conventional duplex stainless steels. Attributed to their unique properties that combine the high mechanical strength of ferrite and the excellent corrosion resistance of austenite, SDSSs have found increasing use in broad engineering applications as load carrying structures and components in aggressive environments. For structural structural safety and accurate service life assessment of engineering structures using SDSSs, a better understanding of fatigue damage mechanisms in such materials is required.

Like other dual-phase materials, the SDSSs are characterized by a heterogeneous microstructure. When subjected to external load, interactions at microstructural level may occur, leading to the development of microstresses. Such microstresses can be classified as phase stresses and intergranular stresses, depending on their origins. The former are attributed to differences in phase properties and are induced to accommodate the strain incompatibility between the austenite and the ferrite. The intergranular stresses which are often found in plastically deformed materials with a strong texture are generated because of elastic and plastic anisotropy associated with the preferred grain orientation distributions. As a result of the micromechanical interactions, both stresses and strains are not uniformly distributed at microstructural level. The actual load sharing on

* Correspondent author

microscopic scale is, therefore, dependent on the phase-property mismatch, microstructural features and residual stresses which exist unavoidably in two-phase materials.

The importance of the micromechanical interactions for the macroscopic behaviour of polycrystalline materials is well recognized ([1] - [5]). The microscopic load sharing in single as well as two-phase materials has been experimentally and theoretically studied for the influence of uniaxial static loading. It has been demonstrated that microstresses develop under the applied load and result in load transfer between the phases as well as between grain subsets of different orientations ([1], [4] and [5]). As for the fatigue behaviour of dual phase materials, published research work has been focused more on the interactions between microstructural features such as phase/grain boundaries and fatigue cracks ([6] - [8]). Few publications deal with the development of microstresses or microscopic load sharing during cyclic loading and their influence on the fatigue behaviour, see, however, references [9] - [11]. For steel 1080 with spheroidized microstructure of cementite and ferrite, while the residual microstresses fade rapidly during fatigue, the more stable residual macrostresses were found to strongly affect crack initiation behaviour ([10]). On the other hand, for duplex stainless steel SAF 2304 consisting of austenite and ferrite, the residual microstresses were observed to increase with pulsating stress-controlled fatigue loading, which was associated with the rapid hardening of austenite ([9]). The cyclic loading response of the material was thus mainly controlled by the plastic behaviour of the austenitic phase ([9]). Knowledge of the residual stress stability and microscopic load partitioning during cyclic loading is essential for understanding the fatigue behaviour of materials. An accurate analysis of integral structural life is possible only when the role of residual stresses and microstructure induced stress heterogeneity is considered.

This paper is part of a project which is aimed at understanding fatigue damage mechanisms in duplex stainless steels and the influence of microstructural and stress heterogeneity typical for such steels. In the current work the micromechanical behaviour of a superduplex stainless steel of grade SAF 2507 (UNS S32750) was investigated by experiment and simulation. The neutron diffraction technique was employed to study the development of residual lattice strains at the different cyclic deformation stages, the analysis of which provides insights into the inter-phase and intergranular reactions under cyclic loading. In addition, simulation by a Visco-Plastic Self-Consistent (VPSC) model was carried out to elucidate the development of macrostresses and phase stresses at the cyclic hardening stage. The results will provide voluble input to the development of fatigue model to simulate the cyclic behaviour and predict the fatigue life of duplex stainless steels.

MATERIAL AND EXPERIMENTS

Material and fatigue test

A hot rolled Φ20 mm bar of SAF 2507 steel was used in this study. The chemical composition of the steel is (in weight percentage): 25 Cr, 7 Ni, 4 Mo, 1.2 Mn, 0.8 Si, and 0.3 N. It was received in solution-annealed and quenched condition. The 0.2% proof strength and tensile strength derived from the tensile test shown in Fig. 1 is 606 MPa and 830 MPa, respectively. The microstructure of the as-received material is shown in Fig. 2. It consists of 42% ferrite (α) and 58% austenite (γ) in volume. Neutron diffraction measurements reveals that texture in the γ-phase mainly consists of a {100}<001> component ({hkl}//ND and <uvw>//RD)) and a weak fiber component with <111>//RD [6]. RD is the rolling direction and TD and ND refer to two perpendicular radial directions. The texture in the α-phase is stronger and dominated by a {110}<001> component. A weak <111> -fiber texture is also found.

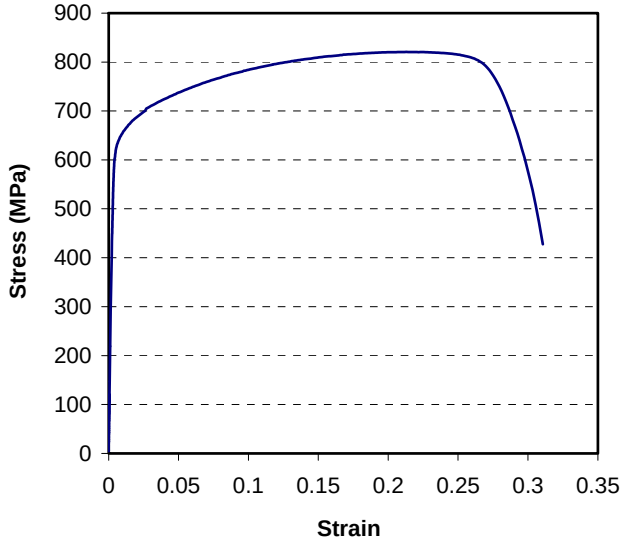

Figure 1. Stress-strain curve from tensile test.

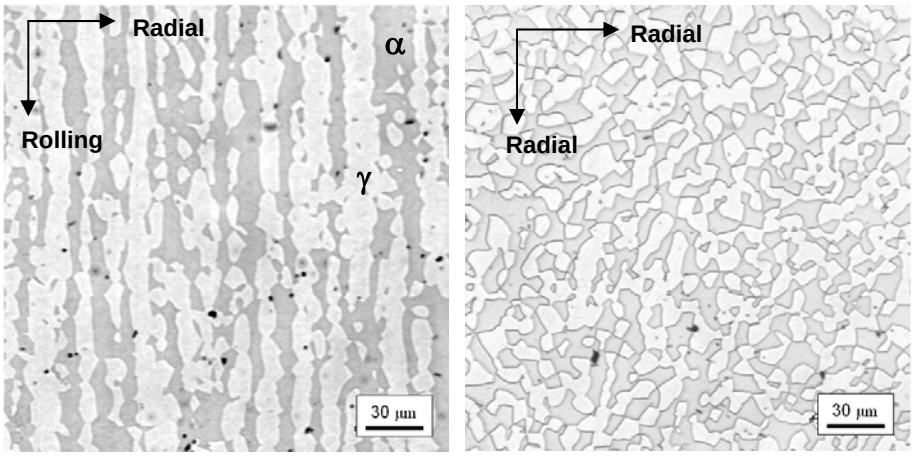

Figure 2. Micrographs showing the constituent phases in the superduplex stainless steel.

Fatigue specimens with a 10 mm diameter gauge section were machined from the hot rolled bar. The surface of the gauge section was polished using P4000 polishing paper with diamond paste. The low cycle fatigue tests were performed under total strain control using a computer controlled servo-hydraulic 100 kN Instron machine at room temperature. The strain was measured using an extensometer with a gauge length of 25 mm. A symmetric push-pull mode with a strain amplitude of 0.5×10^{-3}, a sinusoidal waveform and a cyclic strain rate of $3*10^{-5}$/s was applied. The fatigue test was started with a tensile stress and stopped when the total strain returned to zero. Four specimens were unloaded to zero stress after reaching 1, 10, 100 and 3000 cycles, respectively. These specimens were then used in the neutron diffraction experiments to study the evolution of residual lattice strains. The cyclic deformation behaviour of the steel exhibits typically three distinct stages: initial hardening, softening and saturation before fracture occurs, as can be seen in Fig. 3.

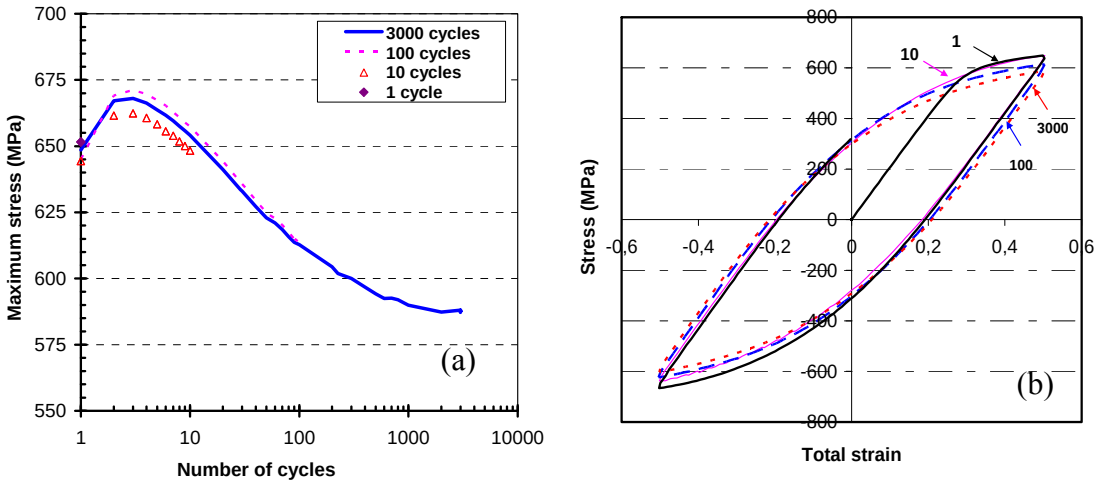

Figure 3. Cyclic softening curves for the specimens tested with Δε/2=0.5%.

Stress-induced transformation of austenite has not been investigated in this study. However, as the SAF 2507 is rather stable, it is believed that such transformation is unlikely to occur under cyclic plastic deformation.

Diffraction experiments

The principle of neutron diffraction stress measurement is rather straightforward. By neutron diffraction, interplanar spacings of the stressed specimens for a particular *hkl* plane, d_{hkl}, are determined. Residual lattice strains (elastic) are then calculated through the following equation:

$$\varepsilon_{hkl} = \frac{d_{hkl} - d_{hkl,0}}{d_{hkl,0}} \tag{1}$$

For the stress-free reference, $d_{hkl,0}$, we used the values which were determined in [5]. Once the elastic strains are obtained for certain specimen directions, the corresponding residual stresses can be derived via Hooke's law [12]. The stresses obtained directly from diffraction measurements are the phase-specific stresses, which are the sum of macrostresses and microstresses.

The neutron diffraction experiments were carried out on the dedicated neutron diffractometer for stress and texture analysis at the Studsvik Neutron Research Laboratory in Sweden. A double focusing Si-(331) monochromator was used to provide a monochromatic neutron beam with a nominal wavelength of 1.7 Å. Residual lattice strains were investigated for the (200), (220) and (311) planes of the austenitic phase and the (200) and (211) planes of the ferritic phase. Table 1 gives their elastic constants which are derived from the single crystal elastic constants of austenite and ferrite ([13] and [14]) using Kröner model. The strain measurement direction was determined by an azimuth angle ϕ and a tilting angle ψ defined within each ϕ-plane (Fig. 4). Mapping was made to cover the axial and radial directions for 5 ϕ-planes with 10° interval. The gauge volume for the strain mapping, which was centred at the specimen axis, is defined by both the incident and diffracted beam slits. They are 3.5 mm wide in the scattering plane and 3.5 mm high out of the scattering plane.

TABLE 1 Elastic constants for the austenite and ferrite planes

	γ-(200)	γ-(220)	γ-(311)	α-(200)	α-(211)
E (GPa)	152	211	184	181	228
ν	0.33	0.264	0.294	0.321	0.275

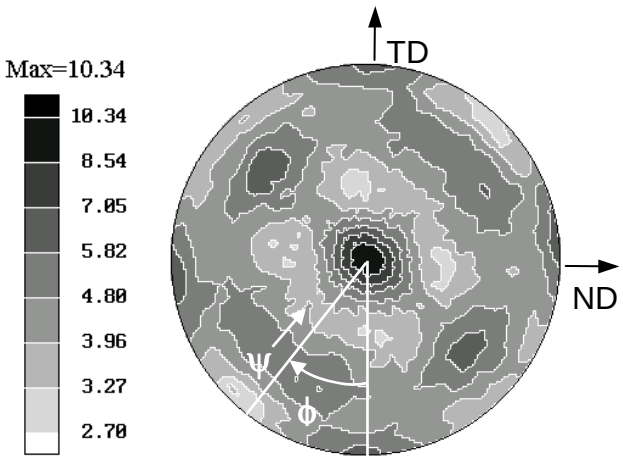

Figure 4. The γ-{200} pole figure. ϕ and ψ define the strain measurement directions.

SIMULATION

A two-phase Visco-Plastic Self-Consistent (VPSC) model was adapted to simulate the micromechanical behaviour of the duplex steel under cyclic loading. In this model, the interactions between grains/phases are derived by considering each grain as an inclusion embedded in a homogeneous medium equivalent to the microstructural constituent of the duplex steel. The model had been successfully applied to uniaxial loading of duplex stainless steel [15]. While a brief account of set-ups for the present simulation is given below, a more detailed description of the model can be found in [15]. In the present simulation, 2592 and 1877 ellipsoidal inclusions (with the axes ratio of 1:1:3 corresponding to ND, TD and RD) representing grains of austenite (58%) and ferrite (42%), respectively, were included. The initial orientation distributions of the grains were set according to the experimental textures. For the austenitic phase with fcc crystal structure, plastic deformation was considered to be caused by slip on the close-packed {111}<110> system. For the bcc ferritic phase, slip was considered to take place on the {110}<111> and {112}<111> systems. By controlling the incremental strain tensor ε_{ij}, one loading cycle is applied in three steps: 0 to 0.5%, 0.5% to -0.5% and -0.5% to 0%. As the mechanism for cyclic softening is not implemented in the model, it is applicable only to the initial cyclic hardening stage. In this paper, results of the first loading cycle are presented and compared to the neutron diffraction measurements.

RESULTS AND DISCUSSION

Evolution of residual stresses by neutron diffraction experiment

The measured residual lattice strains, ε_{hkl}, are plotted as a function of $\sin^2\psi$ in Fig. 5 to 9. All data shown are averages over all the measured ϕ-planes. Before the cyclic loading all the investigated *hkl* planes display a reasonable linear ε-$\sin^2\psi$ distribution (Fig. 5), suggesting a negligible influence of plastic anisotropy. The essentially positive residual strains indicate the existence of residual macrostresses in the specimen. Strain scans across a specimen radius using a smaller gauge volume and the α-(211) and γ-(311) planes have indeed revealed tensile axial stresses in the centre and compressive axial stresses in the outer diameter of the specimen. This characteristic residual stress field arises from different cooling rates between the centre and the surface layer when the hot rolled bar was quenched in water after solution-annealing treatment. Using the Hooke's law and the elastic constants in Table 1, axial stresses were determined from the elastic strains given in Fig. 6. The phase-specific residual stress, averaged over all the *hkl* planes for the respective phases, is found to be 356 MPa in the austenite and 141 MPa in the ferrite. The larger thermal expansion coefficient of the austenite than the ferrite leads to tensile microstresses in the former and compressive in the latter.

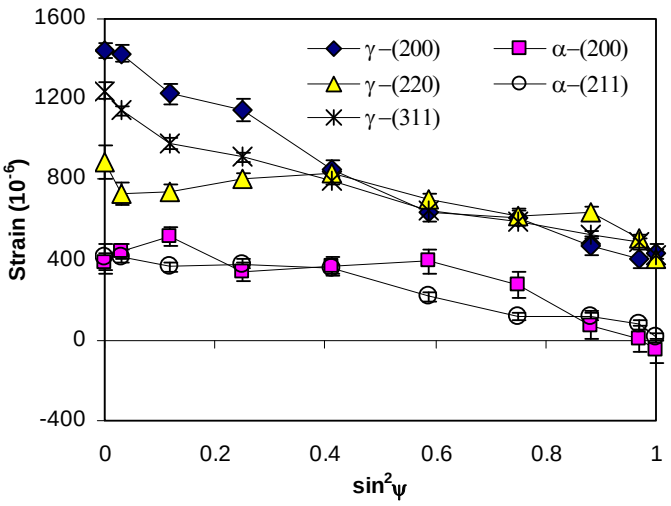

Figure 5. Residual lattice strains in the as-received condition.

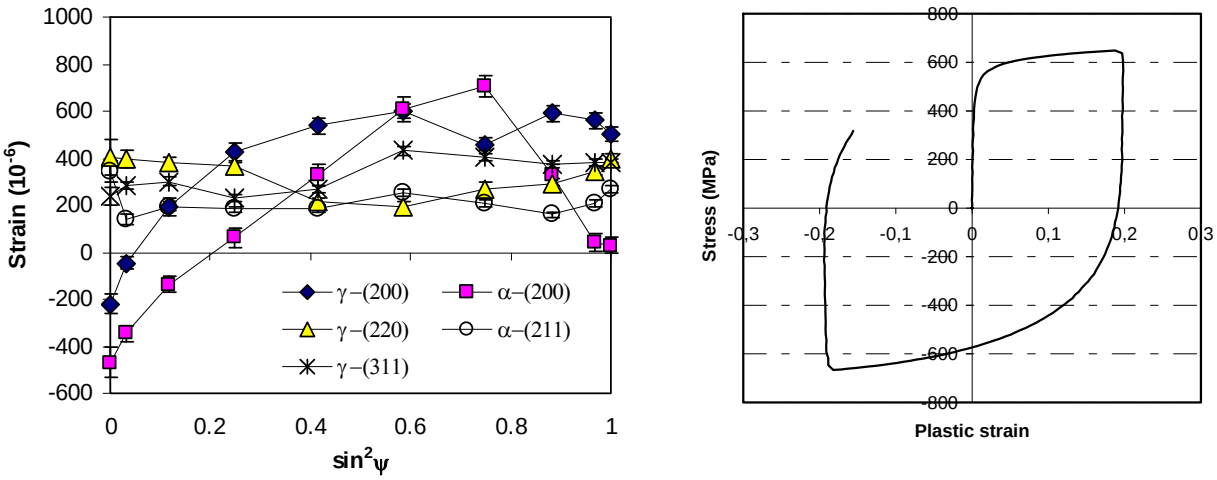

Figure 6. Residual lattice strains after the first loading cycle (left) and the corresponding hysteresis loop (right).

Both the strain magnitude and the shape of the ε-$\sin^2\psi$ curves change significantly in the unloaded specimens, which indicate a strong influence of cyclic loading on the residual micro- and macrostresses. Already after the first loading cycle, a large difference between different *hkl* planes is observed in both the austenite and the ferrite (Fig. 6). In particular the non-linear strain distribution for the γ-(200) and α-(200) planes signifies the generation of grain-orientation-dependent residual stresses. Because of plastic anisotropy, strong intergranular interactions occur under loading, leading to a non-homogenous distribution of microstresses among grains of different orientations. The intergranular stresses remain as residual stresses after unloading. It can be inferred by comparing Fig. 7-9 to Fig. 6 that subsequent cycling seems to have a smaller effect on the grain-orientation-dependent stresses. The difference between *hkl* planes for the respective phases decreases very slightly after 10 cycles (Fig. 7) but increases again in the specimen unloaded from 100 cycle. Cyclic loading from 100 to 3000 cycles causes very little changes in the shape of the strain curves (Figs. 8 and 9).

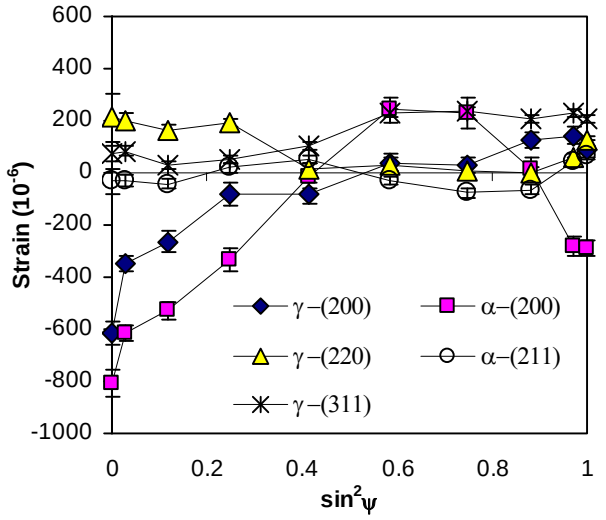

Figure 7. Residual lattice strains after 10 cycles.

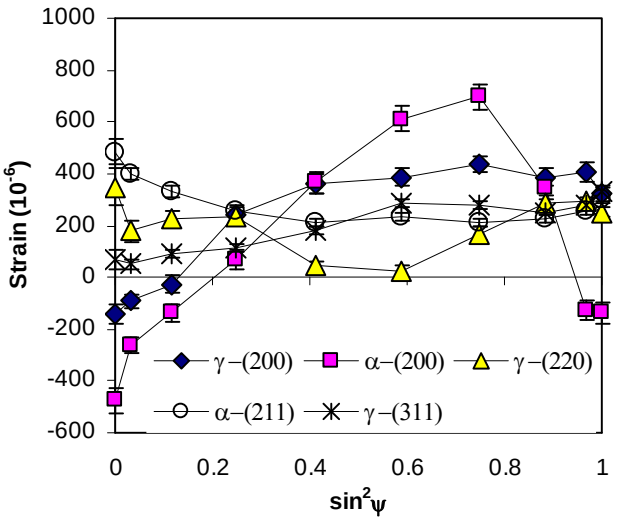

Figure 8. Residual lattice strains after 100 cycles.

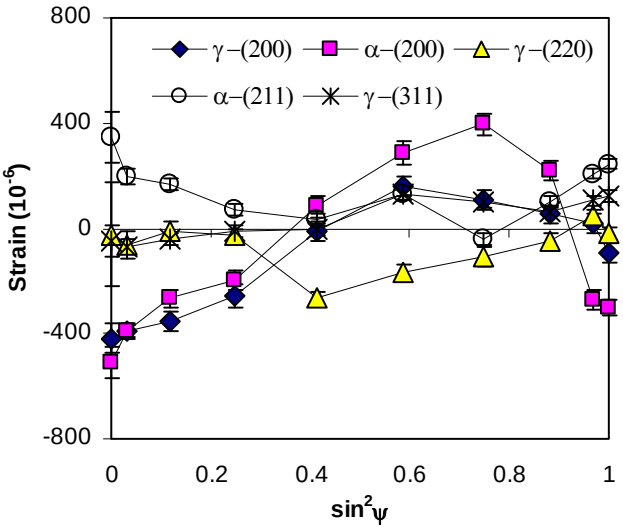

Figure 9. Residual lattice strains measured after 3000 cycles.

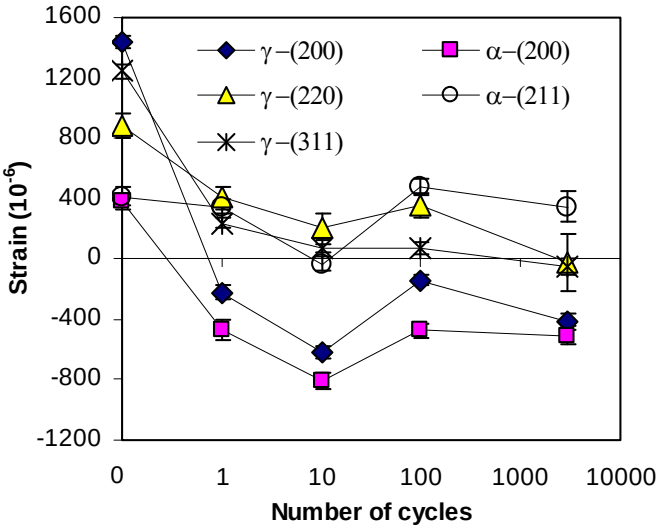

Figure 10. Axial residual lattice strain evolution with increasing loading cycles.

cycles, the axial strain is essentially relaxed for the γ-(220) and (311). The α-(211) retains a tensile strain while the α-(200) and γ-(200) have a compressive strain.

Stress analysis to separate the residual macrostresses and microstresses was performed for measurements using the α-(211) and γ-(311) planes, both of which are less sensitive to grain-orientation-dependent stresses and show a reasonable linear ε-$\sin^2\psi$ curve. On the assumption of a linear distribution, linear regression analysis was performed on the experimental ε-$\sin^2\psi$ distribution, from which the axial and transverse strains, ε_a and ε_r, were obtained at $\sin^2\psi = 1$ and 0, respectively. The phase-specific axial and transverse stresses, σ_a and σ_r, for a phase i were then calculated from the strains using the following equations:

$$\sigma_a^i = \frac{E}{1+\nu}\left[\varepsilon_a^i + \frac{\nu}{1-2\nu}(\varepsilon_a^i + 2\varepsilon_r^i)\right] \tag{2}$$

$$\sigma_r^i = \frac{E}{1+\nu}\left[\varepsilon_r^i + \frac{\nu}{1-2\nu}(\varepsilon_a^i + 2\varepsilon_r^i)\right] \tag{3}$$

where E and ν, whose values are given in Table 1, are the Young's modulus and Poisson's ratio, respectively, for the hkl-plane in concern. Considering the elastic equilibrium, the residual macrostresses are the volume-weighted average of the phase-specific stresses, σ^α and σ^γ:

$$\sigma_{Macro} = \sigma^\alpha V^\alpha + \sigma^\gamma V^\gamma \tag{4}$$

The residual microstresses for phase i is:

$$\sigma_{Micro}^i = \sigma^i - \sigma_{Macro} \tag{5}$$

The calculated stress values are presented in Table 2. Their uncertainty which is also given in Table 2 was derived from the standard deviation of the axial and transverse strains obtained from the linear regression analysis mentioned above. It can be seen that an almost complete relaxation of the thermal residual macrostresses is reached after 3000 cycles. The thermal residual microstresses, which are tensile in the austenite and compressive in the ferrite, decrease with increasing number of loading cycles. After 100 cycles, compressive microstresses are found in the austenitic phase, which are balanced by tensile microstresses in the ferritic phase. Cyclic loading into the saturation stage has little impact on the phase stresses which are the microstress discrepancy between the phases.

The diffraction peak width, given as Full Width at Half Maximum intensity (FWHM), is plotted in Fig. 11 as a function of loading cycles. It is averaged over all the measurement directions for respective *hkl* planes. For a given diffraction set-up and material condition, any variation of the peak width during loading indicates changes in inhomogeneous elastic strains and defect densities within the diffraction volume. In this case, the variation of FWHM observed can be interpreted as the influence of cyclic loading on the dislocation density or residual stress gradient. Obvious decrease of the FWHM is observed for both phases in the specimen unloaded after 1 cycle. This initial drop can be explained by the reduction of a large macroscopic stress gradient by the first loading cycle. The peak width of the ferrite continues to decrease in subsequent cycling but increases from 10 cycles for α-(211) and 100 cycles for α-(200). For the austenite, the peak width is almost constant up to 100 cycles. It then increases slightly at the saturation stage. Such phase-dependent changes can be related to the different cyclic behaviour that the ferrite has a larger cyclic softening rate than the austenite [16].

TABLE 2 Residual stresses (in MPa) derived from α-(211) and γ-(311) lattice strains

Number of load cycles	Phase-specific stress		Phase-specific stress		Macrostress		Microstress			
	α-(211)		γ-(311)				α-(211)		γ-(311)	
	σ_a	σ_r	σ_a	σ_r	σ_a	σ_r	σ_a	σ_r	σ_a	σ_r
0	140 (12)	71 (8)	361 (16)	259 (13)	268 (11)	180 (8)	-128 (12)	-109 (9)	93 (8)	79 (6)
1	109 (19)	108 (13)	144 (13)	165 (10)	129 (11)	141 (8)	-20 (13)	-33 (8)	15 (10)	24 (7)
10	-6 (16)	0 (11)	61 (11)	88 (9)	33 (9)	51 (7)	-39 (11)	-51 (7)	28 (8)	37 (6)
100	153 (21)	126 (15)	81 (15)	117 (9)	111 (10)	121 (8)	42 (14)	5 (6)	-30 (10)	-4 (7)
3000	76 (34)	65 (24)	12 (9)	37 (7)	39 (15)	49 (11)	37 (20)	16 (8)	-27 (15)	-12 (12)

* σ_a and σ_r refer respectively to the axial and transverse stresses. Estimated uncertainties in stress are given inside brackets.

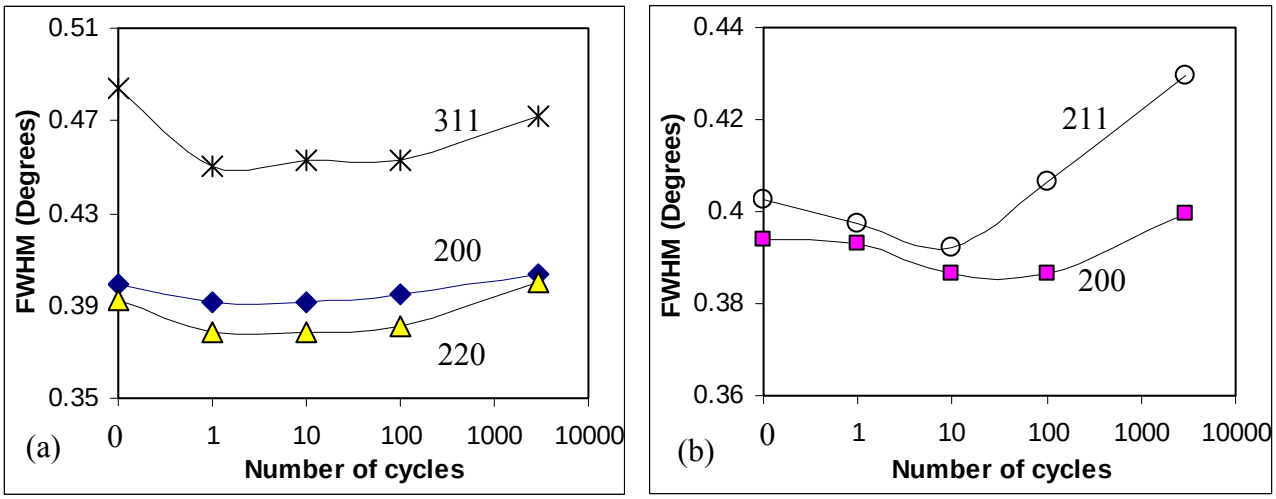

Figure 11. Diffraction peak (FWHM), averaged over all the measurement directions, for austenite (a) and ferrite (b).

Micromechanical behaviour under cyclic loading

In order to introduce into the model the initial residual stress field found in the specimen before fatigue loading, a thermal process with temperature gradient corresponding to water quenching following the solution treatment was modelled to generate thermal microstresses in the respective phases. In addition, the thermal macrostress determined from the neutron diffraction measurement

was imposed on both phases. Some material parameters needed for the simulation were determined from fitting the model to the tensile stress-strain curve given in Fig. 1, assuming no residual macrostresses as its integration over the cross-section is zero.

The calculated residual stresses before and after the first loading cycle are presented in Table 3. As can be seen, changes in the residual stresses caused by the first loading cycle are well predicted by the model. Based on the good agreement between the experiment and the simulation, both macroscopic and microscopic behaviour predicted by the model will be explored below.

TABLE 3 Simulated residual stresses (in MPa)

Number of load cycles	Phase-specific stress		Phase-specific stress		Macrostress		Microstress			
	α-(211)		γ-(311)				α-(211)		γ-(311)	
	σ_a	σ_r	σ_a	σ_r	σ_a	σ_r	σ_a	σ_r	σ_a	σ_r
0	145	147	361	206	270	180	-125	-33	91	26
1	118	114	197	169	164	146	-46	-32	33	23

Fig. 12 shows how the simulated axial macrostress (the sum of the applied stress and the axial residual macrostress) in the duplex steel varies with applied strain during the different loading stages of the cycle. The simulated phase-specific stress in the axial direction is also plotted in the same figure for both the austenite and the ferrite. Because of the thermal residual stresses, loading starts from certain stress values. While the residual macrostress places both phases in tension, the thermal residual phase stress leads to a larger stress in the austenite than in the ferrite. With increasing deformation in stage 1 (0 to 0.5% strain) the microstress discrepancy of thermal origin remains between the phases, which, however, decreases when the applied strain reaches about 0.14%. At this point, yielding starts in the austenite, causing load transfer from the austenite to the ferrite. Further straining to 0.4% induces plasticity even in the ferrite, upon which the phase stress starts to increase again. Stress redistribution occurs with load transfer from the ferrite back to the austenite because the latter has the larger strain hardening rate. The stronger hardening tendency of the austenite is clearly identified with its prominently larger slope in the figure. At the end of stage 1 (0.5% strain), the microstress partitioned between phases becomes 100 MPa, which is much smaller than the initial phase stress of 216 MPa. It can be concluded that the thermal residual microstresses are largely relaxed by the phase interactions characterised by plastic deformation in the austenite.

During stage 2 both phases are first unloaded elastically from their respective maximal tensile stress and then loaded again but in compression after that the applied strain reaches zero. At -0.05% strain, yielding appears in both phases. The elastic interaction between the phases leads to a somewhat larger phase stress before the plastic flow. With increasing plastic deformation, the phase stress decreases slightly due to a different strain hardening behaviour between the two phases. At the maximal applied strain, the phase stress is about 100 MPa.

Essentially elastic behaviour is found for the last stage of the loading cycle. The phase stress decreases somewhat during unloading to the zero applied strain, attributed to the elastic interaction between the austenite and the ferrite. A large tensile stress of 490 MPa remains in the duplex steel at the end of the first loading cycle. To compare with the neutron measurements which were carried out at zero external stress, an additional unloading process was applied to simulate removal of the

specimen from the fatigue testing machine. The specimen was then unloaded to a stress determined from a simulation carried out on the same specimen without involving the residual macrostress. The unloading was elastic and very little happens to the microstresses. As shown in Table 3, the residual phase stress is 79 MPa.

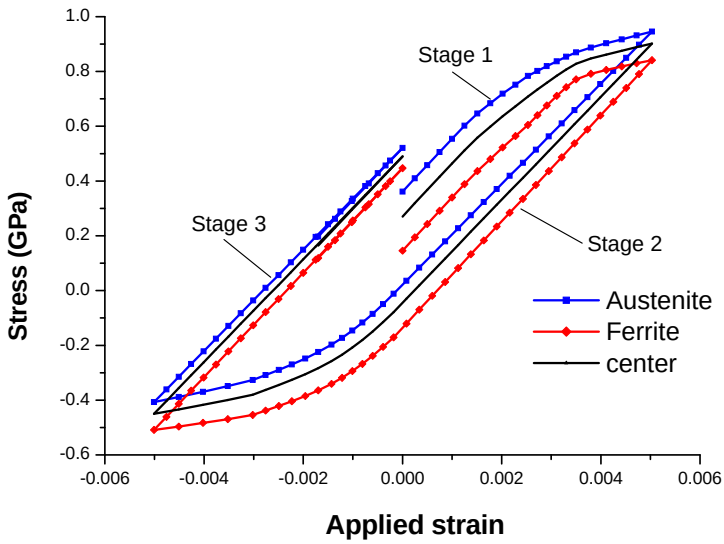

Figure 12. Simulated total stress variation with applied strain for the constituent phases and the duplex steel.

The effect of cyclic loading on the residual macrostress can be inferred by comparing the macrostress-strain curve in Fig. 12 to the applied stress-strain curve in Fig. 6. For a given applied strain, the residual macrostress can be considered as the difference between the two curves. The difference in stress at the end of each loading stage demonstrates that relaxation of the residual macrostress occurs in all the loading stages. It should be pointed out that the current simulation concerns only a sample volume in the centre of the fatigue specimen, which is initially in tension. As aforementioned, the outer region of the fatigue specimen is subjected to compression. Interactions between the regions with different initial macrostresses during loading are expected, the negligence of which means that the simulation give, at the best, a semi-quantitative description of the variation of residual macrostresses. Nevertheless, the results, as demonstrated above, does throw some lights upon the micromechanical interactions in the duplex steel and contribute to our understanding of the micromechanical behaviour, upon which the macroscopic properties of the duplex steel rest.

A couple of interesting points can be made from the above analyses. The measured residual stresses in the unloaded fatigue specimens reveal strong microscopic interactions during cyclic loading of the superduplex stainless steel. The development of phase stresses which changes the microscopic load sharing between the phases is closely related to the differential phase behaviour and initial residual microstresses. Phase interactions of elastic nature, as revealed by the simulation, modify the microscopic load sharing, through which the appearance of plastic deformation in the phases is also shifted. On the other hand, the evolution of the residual microstresses involves microplasticity and the correlations between them are more complicated. For the current steel in its initial state, the austenite is prone to plastic deformation under tension because of its somewhat lower initial hardness [16] and larger tensile microstresses. Yielding, therefore, occurs in the austenite rather earlier in the tensile phase of the loading cycle, leading to the large reduction of

thermal residual phase stresses observed by the neutron diffraction measurements. Plastic flow during the compression loading phase has a much smaller effect on the phase stresses, as both phases yield almost simultaneously. Phase interactions in following cyclic loading leads to further changes in the residual microstresses. As can be seen in Fig. 3, after the initial cyclic hardening stage which extends over 3 loading cycles, the steel becomes cyclic softened. The ferrite which has a higher softening rate eventually becomes the softer phase in the steel [16]. This change in the relative phase properties likely results in the tensile microstresses in the ferrite and compressive microstresses in the austenite in the specimen unloaded from 100 cycles.

In accordance with in-situ neutron experiment of the same steel under uniaxial loading in [5], strong interactions between grain subsets of different orientations occurs during the first loading cycle. Intergranular stresses appear because of strain incompatibility induced by plastic deformation in the respective phases. Once formed, they remain and change somewhat during following cyclic loading. This suggests that the continued cyclic deformation after the initial loading cycle may have little influence on the strain incompatibility which is the origin of intergranular stresses.

CONCLUSIONS

Micromechanical interactions in a superduplex stainless steel SAF 2507 under low cycle fatigue loading were investigated with respect to residual stresses and differential phase property between the austenite and the ferrite. By experiment and simulation, the evolution of residual stresses with cyclic loading was analysed and correlated to the deformation behaviour of the constituent phases. The main findings of the work are summarised below.

Large thermal residual stresses varied both macroscopically and microscopically are found before fatigue loading. The residual macrostresses relax rapidly but not completely with cyclic loading. Microscopically, load transfer occurs during fatigue loading as a result of different residual microstresses and different elastic and plastic properties between the austenite and ferrite. As a consequence of microyielding in the austenite, an almost complete reduction of the initial residual microstresses which was tensile for the austenite and compressive for the ferrite is obtained already after one loading cycle. With continued cycling, low tensile residual microstresses eventually develop in the ferrite and compressive microstresses in the austenite, which may be attributed to changes in the relative phase properties.

Strong interactions between grain subsets were also observed during the first loading cycle, resulting in the generation of residual intergranular stresses. These grain-orientation dependent residual stresses seem to be stable, with a small influence from the subsequent cyclic deformation.

ACKNOWLEDGEMENTS

This work is supported by the Swedish Research Council in the framework of SIDA project (Grant No. 348-2004-3475), the National Natural Science Foundation of China (Grant No. 50471026), the National High-Technology Development Plan of China (Grant No. 2003AA331030), and the National Ministry of Education of China in the framework of the NCET project (NCET-04-0282). This work is also supported by the National Science Foundation International Materials Institutes (IMI) Program with Dr. C. Huber as the Program Director. The author Chai G would also like to acknowledge the support of Mr. Lundström M for this work.

REFERENCES

1. Johansson J, Odén M and Zeng X H (1999). Evolution of the residual stress state in a duplex stainless steel during loading. *Acta mater.,* **47**, 2669-2684.
2. Harjo S, Tomota Y, Lukáš P, Neov D, Vrána M, Mikula P and Ono M (2001). Measurements of thermal residual elastic strains in ferrite-austenite Fe-Cr-Ni alloys by neutron and X-ray diffractions. *Acta mater.*, **49**, 2471-2479.
3. Baczmański A and Braham C (2004). Elastoplastic properties of duplex steel determined using neutron diffraction and self-consistent model. *Acta Mater.* **52**, 1133-1142.
4. Lin Peng R, Gibmeier J, Eulert S, Johansson S and Chai G C (2006). In-situ X-ray diffraction study of load partitioning and microyielding for the super duplex stainless steel SAF2507 (UNS S32750). *Materials Science Forum*, **524-525**, 847-852.
5. Jia N, Lin Peng L, Chai G C, Johansson S, Wang G and Wang Y D (2006). Interactions between the phase stress and the grain-orientation-dependent stress in duplex stainless steel during deformation. *Acta Mater.,* **54**, 3907-3916.
6. Stolarz J and Foct J (2001). Specific features of two phase alloys response to cyclic deformation. *Mater. Sci. Eng.,* **A319-321**, 501-505.
7. Bugat S, Besson J, Gourgues A-F, N'Guyen F and Pineau A (2001). Microstructure and damage initiation in duplex stainless steels. *Mater. Sci. Eng.,* **A317**, 32-36.
8. Ankem S, Margolin H, Green C A, Neuberger B W and Gregory Oberson P (2006). Mechanical properties of alloys consisting of two ductile phases. *Progress in Materials Science,* **51**, 632-709.
9. Johansson J and Odén M (2000). Load sharing between austenite and ferrite in a duplex stainless steel during cyclic loading. *Metall. Mater. Trans. A.*, **31A**, 1557-1570.
10. Winholtz R A and Cohen J B (1992). Changes in the macrostresses and microstresses in steel with fatigue. *Mater. Sci. Eng.*, **A154**, 155-163.
11. Almer J D, Cohen J B and Moran B (2000). The effect of residual macrostresses and microstresses on fatigue crack initiation. *Mater. Sci. Eng.*, **A284**, 268-279.
12. Noyan I C and Cohen J B (1987). *Residual Stress – Measurement by Diffraction and Interpretation*. Springer-Verlag, New York.
13. Ledbetter H M (1984). Monocrystal-polycrystal elastic constants of a stainless steel. Phys. Stat. Sol. A, **85**, 85-89.
14. Simmons G and Wang H (1971). *Single Crystal Elastic Constants and Calculated Aggregate Properties: a Handbook.* MIT Press.
15. Jia N, Lin Peng R, Wang Y D and Liaw P K (2008). Micro-mechanical behaviour and texture evolution of duplex stainless steel studied by neutron diffraction and self-consistent modeling. *Acta Mater*., **56**, 782–793
16. Chai G and Lilleback R (2006). Damage and crack initiation behaviour of duplex stainless steel during cyclic loading. *Key Eng. Mater.,* **324-325**, 1117-1122.